THE JOURNAL OF PHYSICAL CHEMISTRY LETTERS
A JOURNAL OF THE AMERICAN CHEMICAL SOCIETY

pubs.acs.org/JPCL

Letter

Cesium-Coated Halide Perovskites as a Photocathode Material: Modeling Insights

Sina G. Lewis, Dibyajyoti Ghosh, Kevin L. Jensen, Daniel Finkenstadt, Andrew Shabaev, Samuel G. Lambrakos, Fangze Liu, Wanyi Nie, Jean-Christophe Blancon, Liujiang Zhou, Jared J. Crochet, Nathan Moody, Aditya D. Mohite, Sergei Tretiak,* and Amanda J. Neukirch*

Cite This: *J. Phys. Chem. Lett.* 2021, 12, 6269−6276

Read Online

ACCESS | Metrics & More | Article Recommendations | Supporting Information

ABSTRACT: Photocathodes emit electrons when illuminated, a process utilized across many technologies. Cutting-edge applications require a set of operating conditions that are not met with current photocathode materials. Meanwhile, halide perovskites have been studied extensively and have shown a lot of promise for a wide variety of optoelectronic applications. Well-documented halide perovskite properties such as inexpensive growth techniques, improved carrier mobility, low trap density, and tunable direct band gaps make them promising candidates for next-generation photocathode materials. Here, we use density functional theory to explore the possible application of pure inorganic perovskites ($CsPbBr_3$ and $CsPbI_3$) as photocathodes. It is determined that the addition of a Cs coating improved the performance by lowering the work function anywhere between 1.5 and 3 eV depending on the material, crystal surface, and surface coverage. A phenomenological model, modified from that developed by Gyftopoulos and Levine, is used to predict the reduction in work function with Cs coverage. The results of this work aim to guide the further experimental development of Cs-coated halide perovskites for photocathode materials.

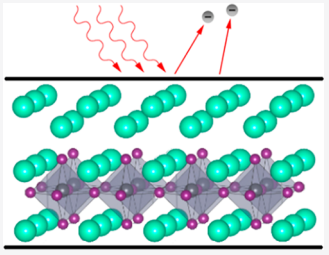

Photocathodes find many uses in satellites, communications,[1] medical imaging,[1,2] energy conversion,[3] and fundamental scientific research.[4,5] Many efforts to improve cathode properties focus on their application in X-ray free-electron lasers (XFELs). These devices promise advances in understanding the physicochemical processes during materials synthesis and characterizing transient states of matter by offering unique probes in biology, chemistry, materials science, and physics.[6,7] However, XFELs also have demanding requirements necessitating photocathodes to produce high-brightness electron beams paired with a high quantum efficiency (QE) in the visible spectrum. Gallium nitride (GaN) is a promising material with a high QE (40%) that was found to be resistant to vacuum contamination,[8] yet its wide band gap of 3.4 eV requires it to be driven with UV light, reducing the available power output.[5,8] Much attention has been paid to alkali-antimonide materials, such as Cs_3Sb, which exhibit threshold emission and high QE but are not very thermally stable and typically contain rough surfaces that limit the achievable mean transverse energy.[4,9] Additionally, alkali-based photocathodes are deposited by expensive, slow, high-temperature methods such as vapor deposition or molecular beam epitaxy.[8,10] The choice of the photocathode is dictated by the specific application at hand. There will assuredly be a trade-off between quantum efficiency vs lifetime/stability vs response time vs emittance. It is generally accepted that the next generation of high-brightness electron-emitting cathodes requires the development of a device with high QE, inexpensive fabrication methods, and the ability to operate under moderate vacuum conditions.[11,12]

Perovskite materials can potentially be candidates for the next generation of photocathodes. Promising results were demonstrated for perovskite oxides, with the formula ABO_3 where A and B are cations.[13−16] Moving away from oxides, lead halide perovskites, in particular, ABX_3, where B is Pb and X is a halide, have been recently studied extensively and have shown a lot of promise for optoelectronic applications such as solar cells,[17] photodetectors,[18,19] and light-emitting diodes (LEDs).[17,20] This is largely due to high carrier mobility,[21,22] low trap density,[23,24] and a tunable band gap.[25,26] With the additional development of inexpensive solution growth methods,[27−29] perovskites have experienced large leaps in photovoltaic power conversion efficiency (PCE). Starting from a value of about 3% in 2009, recent reports in 2018 demonstrate a PCE exceeding about 23%, an increase by a factor of 8 over the past decade.[30−32] Since then, there have been other studies that show perovskite materials for use in water splitting and hydrogen evolution.[33−35] Although not as extensively studied for photocathodes as perovskite oxides,

Received: May 1, 2021
Accepted: June 26, 2021
Published: July 1, 2021

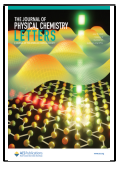

https://doi.org/10.1021/acs.jpclett.1c01412
J. Phys. Chem. Lett. 2021, 12, 6269−6276

Crespo-Quesada et al. demonstrated that these properties and the promise that halide perovskites have shown in other fields are potentially transferable to photocathodes.[36] In order to lower the work function into the optical region for more affordable operating conditions, one technique is to add a coating of Cs. Indeed, recently reported efficient free-electron emission halide perovskite thin films operating in the visible to the ultraviolet spectral range for the first time[37] further motivate in-depth computational studies on this emergent application.

Here we use density functional theory (DFT) to investigate the photocathode performance of Cs-coated halide perovskites. Many current photocathodes utilize Cs coatings to lower the work functions of photocathode materials due to the low electron affinity of Cs.[37−39] In this study, we specifically focus on Cs-coated $CsPbX_3$, where X is a halide (Br or I). We consider the influence of surface termination, coating thickness, and material composition on the work function, electronic and optical properties, and Cs adsorption energy of these perovskites. It has been demonstrated that Cs Pb perovskite thin films are more thermodynamically stable than those that contain MA, and thus this work will focus on $CsPbBr_3$ and $CsPbI_3$.[40] We find high work functions, of around 4 eV, for pristine $CsPbX_3$ (X = I, Br), in agreement with experiment.[41−44] The Cs coating significantly reduces the work function from ∼4 eV to between 1.8 and 2.3 eV, depending on the specific surface termination of the perovskites. The value of the work function depends on the chemical composition of the material, the surface termination, and the surface coverage. In order to predict how to tune the work function, a phenomenological model based on one developed by Gyftopoulus and Levine (GL)[45−47] is used for the development of future systems. Finally, we calculate the formation energy of the Cs coating and Br and I perovskite surfaces. This study should work as a guide toward further experimental development of Cs coated halide perovskites as possible next-generation photocathode materials.

From this work, as well as the work on perovskite oxides by Jacobs et al. and Zhong and Hansmann, we recognize that the work function is extremely sensitive to a variety of structural and calculation parameters.[13,48] Therefore, each source of error is carefully considered and quantified for our simulations. Kohn−Sham wave functions are expanded into a plane wave basis. Information on the energy cutoff, K-point mesh, vacuum spacing between the slabs, and slab thickness is given in the SI (Figures S1−S3 and Table S1). Overall, we correctly capture the range of experimental values reported for the work function and band gap of the bare $CsPbX_3$ and thus expect our values for the Cs-coated surface to likewise be largely accurate. DFT calculations, using the projector-augmented wave method, are performed with the Vienna Ab Initio Simulation Package (VASP).[49−51] The generalized-gradient approximation of Pardew, Burke, and Ernzerhof (PBE)[52] is used to describe exchange and correlation (XC). We focused on the cubic phase of $CsPbX_3$ (X = I, Br), with the simulation cell of the [001] surface shown in Figure 1a−c and the [110] surface shown in Figure 1d−f. The cell parameters' slab design considerations are described in the SI.

In the case of pure materials, we use the cubic phase of $CsPbX_3$, (X = I or Br) with the simulation cell of the [001] and [110] surfaces as shown in Figure 1a,d (details of slab design are presented in SI). To simulate the Cs-coated surface, we started with 0.5 monolayer (ML)[38] of coverage on the [001] surface of $CsPbI_3$. Two inequivalent adsorption sites have been considered; above the Cs in the perovskites slab and above the I (Figure S4). After geometry optimization, the Cs adsorbed over the I appears to be more stable by 1.5 eV compared to the other absorption configuration. The resulting structure is shown in Figure 1b. We further increased the thickness of the Cs coating to 1 ML of coverage in order to observe the effect of additional Cs.[38] We considered two configurations initially; Cs adsorbed in-plane with the Cs adsorbed over the Pb (on top of the Cs already in the layer (Figure S5a) and Cs adsorbed above the Cs adsorbed over the Pb (Figure S5b)). After optimization, the later configuration with staggered Cs layers, as shown in Figure 1c, is found to be more stable. This staggered layer was used as the initial configuration for further calculations. A similar strategy was used to obtain Cs-coated model $CsPbBr_3$ structures.

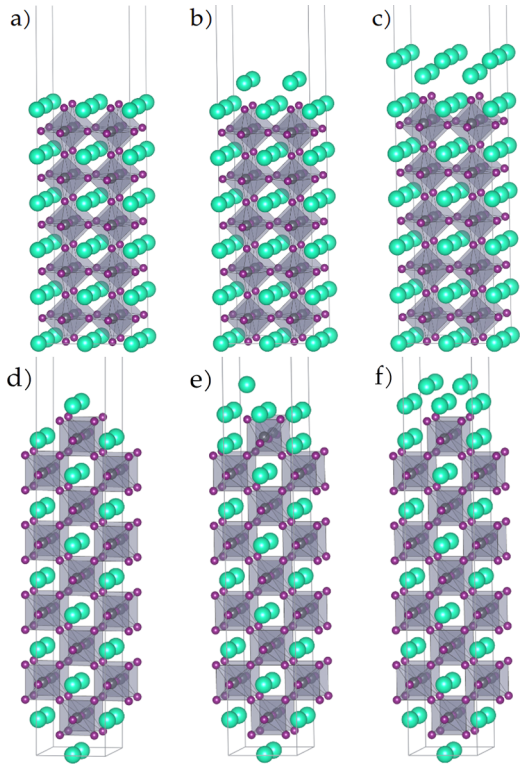

Figure 1. Model of the [001] surface slab of $CsPbX_3$ with (a) no Cs coating, (b) a single coating, and (c) a dense coating (d−f are the same as a−c but for the [110] surface).

Moving to the [110] surface, we kept the previously used Cs coverage density fixed with respect to the [001] surface (Figure 1b,c). The initial starting position of the adsorbed Cs was determined by continuing the underlying lattice structure and further matching the preferential adsorption of Cs over the Pb atoms. The resulting structures used for simulations are shown in Figure 1b,c.

The work function of a material is the minimum energy needed for an electron to escape from the surface of a material to the vacuum, and it plays a dominant role in determining the QE of a photocathode.[5,13] The calculated work function can be expressed as

$$\phi = E_{\text{vacuum}} - E_{\text{Fermi}} \tag{1}$$

where E_{vacuum} is the vacuum energy level and E_{Fermi} is the Fermi energy of the material.[53] A representative graph of the averaged

https://doi.org/10.1021/acs.jpclett.1c01412
J. Phys. Chem. Lett. 2021, 12, 6269−6276

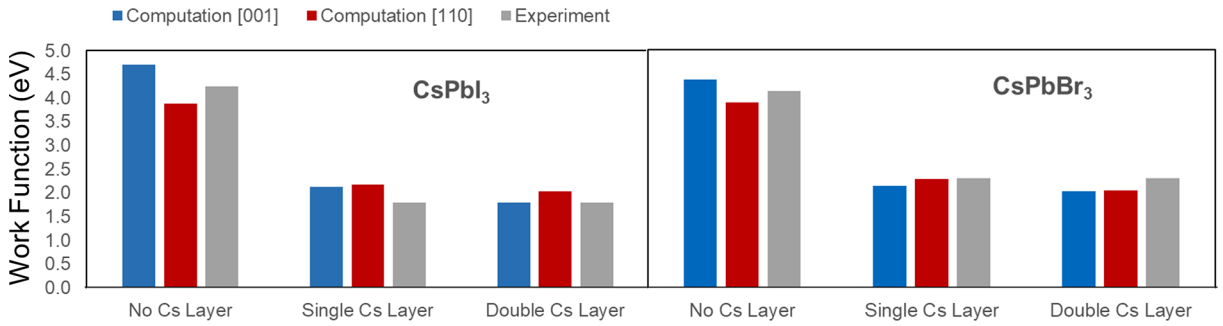

Figure 2. Calculated work functions ϕ of $CsPbX_3$ materials. The experimental value for pristine $CsPbI_3$ was the average value reported in ref 36. The experimental value for pristine $CsPbBr_3$ comes from refs 33 and 34. The experimental values for Cs-coated perovskites are taken from ref 37.

electrostatic potential is shown in Figure S6. The top portion shows the cell being modeled along with which atoms are kept in their bulk positions and which atoms are allowed to optimize. We observe that the electrostatic potential is oscillating within the perovskite slab. However, these oscillations are essentially insensitive to optimization of the surface. In contrast, the vacuum potential does vary with optimization. Before any optimization, the vacuum energy is flat because the system is perfectly periodic. When one side is allowed to optimize to mimic a surface, the vacuum energy becomes different on the sides of the slab. Since we are interested in the surface vacuum energy, the flat part of the dipole-corrected potential closest to the optimized surface provides the value of interest.

Calculated work functions for different materials considered along with available experimental data are summarized in Figure 2. Experimental values for the work function of pristine slabs ranged from 4.1 to 4.4 eV[36] for $CsPbI_3$ and from 4 to 4.3 eV[33,34] for $CsPbBr_3$. Here, the modeled work function of the pristine material closely matches the published experimental values, with the [001] and [110] surfaces representing higher and lower bounds, respectively. This likely points to the fact that the experimental values are an average over the surfaces present in samples. $CsPbBr_3$ has a lower work function than $CsPbI_3$, 4.4 eV compared to 4.7 eV for the [001] surface. However, both $CsPbBr_3$ and $CsPbI_3$ have nearly identical work functions of around 3.88 eV for the [110] surface. The [110] surface of $CsPbX_3$ (X = I, Br) materials is essentially terminated by Cs (Figure 1) and can thus be considered to be partially cesiated. Once a Cs coating is added, we find a significant drop in the work function of anywhere from 1.6 to 2.9 eV compared to the original uncoated systems depending on the specific configuration. This reduction is dominated by the addition of a single Cs layer to the surface (a drop of 1.6 to 2.55 eV). A double Cs layer further lowers the work function by an additional 0.1 to 0.3 eV. In addition, once a coating is added, the work functions on the [110] and [001] surfaces become very similar. Compared to $CsPbBr_3$, the Cs coated $CsPbI_3$ has a slightly lower work function.

A phenomenological model to describe the reduction in work function due to the coverage and surface termination of alkali metals such as cesium, represented as hard spheres, was modified and simplified from a model developed by Gyftopoulos and Levine (GL).[45,46] The GL model successfully predicts the reduction in quantum yield for different wavelengths of metal surfaces with a fractional coverage of cesium.[47,54,55] The coverage is governed by the parameter θ, with $\theta = 0$ being the absence of cesium and $\theta = 1$ being the complete coverage of the surface (a monolayer). In the model work function, $\phi(\theta)$ is composed of an electronegativity term W and a dipole term d:

$$\phi(\theta) = W(\theta) + d(\theta) \tag{2}$$

The foundation and derivation of the GL model are presented in detail in the SI. There is only one scalable parameter, a dimensionless factor f, that is related to the number of coating atoms per unit cell at monolayer coverage. Because the coating atoms need not lie in a plane but can reside on a "rough" surface, the value of f can take values greater than unity. In the results below, f is allowed to vary to achieve measured values of $\phi(\theta = 0.5)$ evaluated using the DFT methods above. Depending on the value of f, a characteristic minimum of $\phi(\theta)$ can occur at submonolayer coverages as shown in Figure S7 for the iconic Cs on W configuration treated by GL. In addition to the fitting parameter f, the covalent radii of the coating atom (cesium) r_c and the substrate atom (Cs or halide) r_w are important input parameters as well.

We applied GL theory to $CsPbI_3$ (Figure 3) and $CsPbBr_3$ (Figure S8). Here the values of $\phi(\theta)$ in Figure 2 were matched to the values of θ = (0, 0.5, 1.0) for both [001] and [110] crystal planes. As shown in Figure 1, different orientations of the crystal faces at the surface bring different atoms to the quincunx on the plane making up the surface. For both the

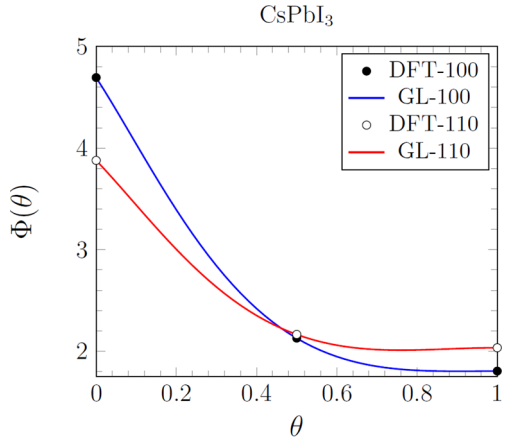

Figure 3. Gyfopoulous–Levine relation for $CsPbI_3$ evaluated using eq (S6) with parameters r_c = 0.230 nm and n = 1 using the values of $\phi(\theta)$ from Figure 2 for the fitted value of f = 1.0127 and r_ω = 0.133 nm for [001] (N_0 = 1) as the quincunx corners are I and f = 0.8197 and r_ω = 0.230 for [110] (N_0 = 2) as the quincunx corners are Cs.

https://doi.org/10.1021/acs.jpclett.1c01412
J. Phys. Chem. Lett. 2021, 12, 6269–6276

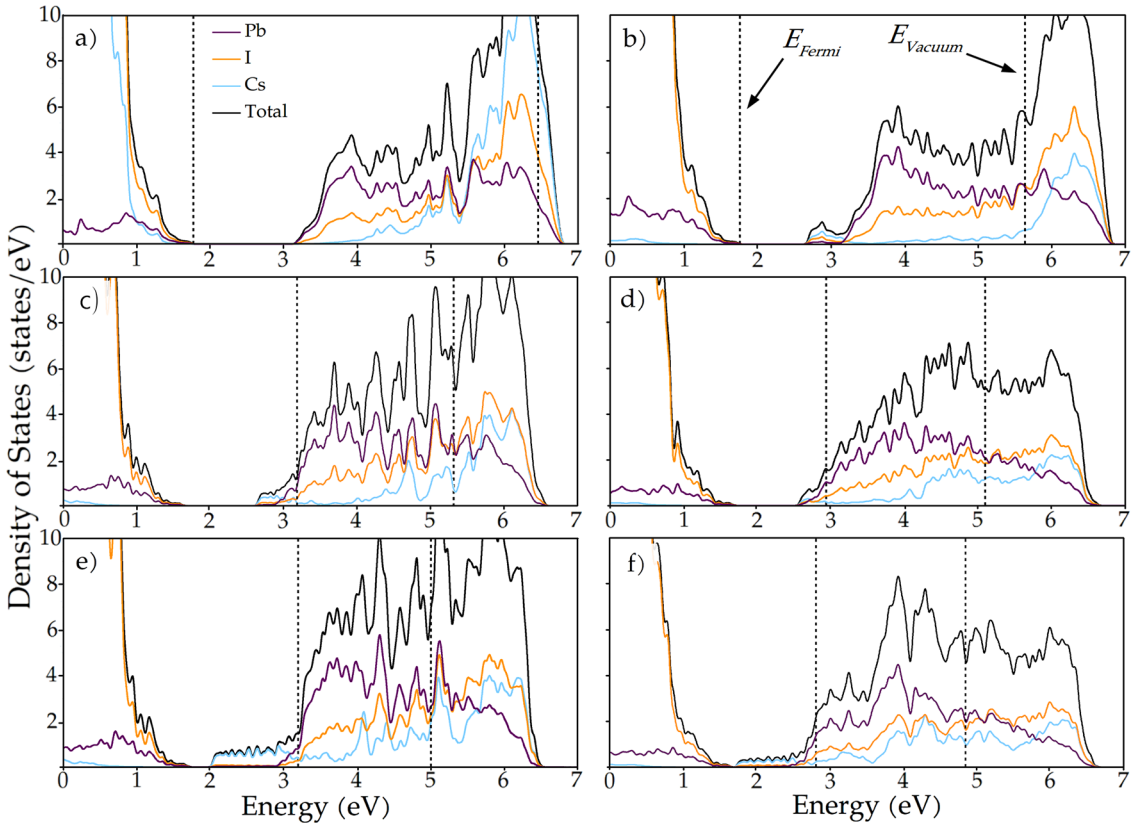

Figure 4. Density of states (DOS) of $CsPbI_3$ for (a) the [001] surface without Cs, (b) the [110] surface without Cs, (c) the [001] surface with a single layer of Cs, and (d) the [110] surface with a single layer of Cs, (e) the [001] surface with a double layer of Cs, and (f) the [110] surface with a double layer of Cs.

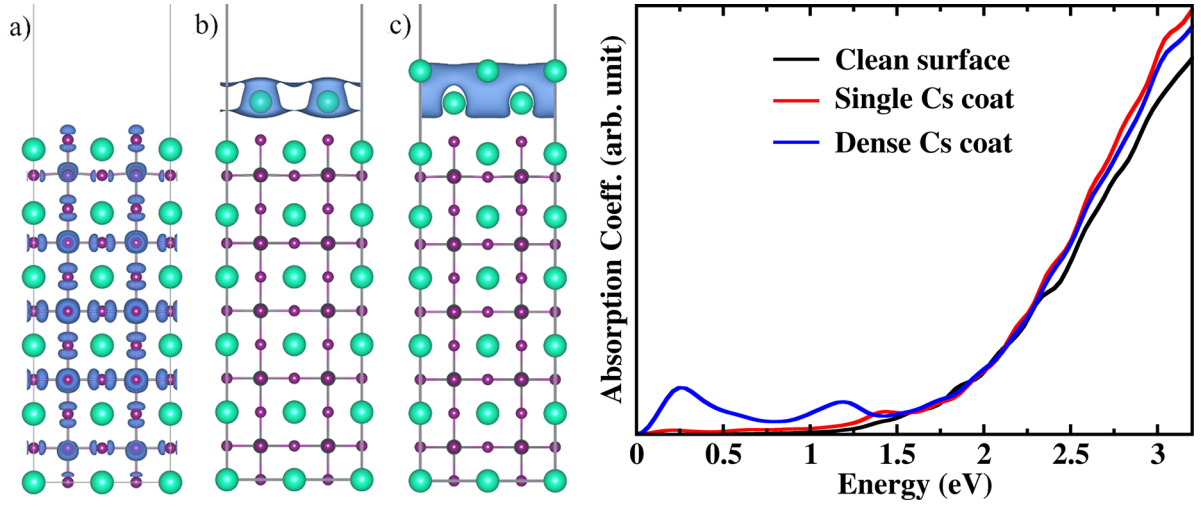

Figure 5. Charge density of the [001] surface for the HOMO of (a) the pure $CsPbI_3$ slab, (b) the $CsPbI_3$ slab with a single Cs layer, and (c) the $CsPbI_3$ slab with a dense layer of Cs. (d) Optical absorption spectra of [001]-terminated $CsPbI_3$ with a clean surface and with a Cs coating. The low-energy peaks are prominent with the dense Cs coating.

[001] and [110] faces, the center of the quincunx is Cs. For the [110] surface, the four corners of the quincunx are also Cs and thus r_w is set to the Cs value. For the [001] surface, the four corners of the quincunx are I or Br, and for this case, r_w is set to the halide value. Clearly, this assignment is subjective as the model was developed for single-species crystals and perovskites are multispecies crystals. However, this is acceptable for phenomenological hard-sphere theory like GL, which can make valuable predictions, such as work function tuning, on-material surface termination, and surface coverage for the experimental design of next-generation photocathodes. For further discussion of the emission of electrons from submonolayer coatings, see refs 46 and 56.

Further insight into what is physically taking place can be ascertained by looking at the partial density of states, charge density, and absorption energy of Cs on a surface. In order to compare the different systems on the same footing, we aligned the Pb:5d states at −15.3 eV. The partial density of states

https://doi.org/10.1021/acs.jpclett.1c01412
J. Phys. Chem. Lett. 2021, 12, 6269−6276

(Figure 4 for $CsPbI_3$ and Figure S9 for $CsPbBr_3$) shows that the dominant contributor to the valence band maximum (VBM) in all cases is the halide, as expected. In pure perovskite systems, the conduction band minimum (CBM) is almost entirely composed of Pb orbitals for the [001] surface (Figure 4a and Figure S9a), but for the [110] surface, a significant portion for the DOS comes from the Cs orbitals. This is another indication of the [110] surface being effectively partially cesiated. There are two main differences in the DOS once a Cs coating is added to the pure perovskite slabs (Figure 4c−f for $CsPbI_3$ and Figure S9c−f for $CsPbBr_3$). Most notably, the Fermi level (and likewise the highest occupied molecular orbital (HOMO)) is raised into the conduction band of the pristine system. Such a major change is responsible for the lowering of the work function. Furthermore, with the addition of surface Cs more occupied Cs edge states appear within the band gap, contributing to the net lowering of the work function.

To illustrate these observations, we displayed the charge density of the HOMO for the [001] surface of pure $CsPbI_3$ (Figure 5a) and the same quantity for systems with one and two monolayers (Figure 5b,c). As expected the charge density of the HOMO in a pure perovskite slab is completely delocalized within the bulk of the material and is spatially located on the I atoms. In contrast, the charge density of the HOMO for the Cs-coated slabs is located completely on the surface Cs atoms. The respective HOMOs for the [110] surfaces of pure and Cs-coated $CsPbBr_3$ shown in Figure S10a−c display a very similar pattern. All charge densities were plotted using a 3×10^{-4} isovalue.

To explore the influence of the Cs coating on the optical properties of these perovskites, we evaluate the frequency-dependent dielectric function within the random phase approximation as implemented by Gajdos et al.[57] Furthermore, the imaginary part of this function was used to calculate the optical spectra of [001]-terminated $CsPbX_3$ (X = I, Br). As shown in Figures 5d and S11, the absorption spectra for clean surface $CsPbI_3$ exhibit its semiconducting nature with the absorption edge appearing at 1.5 eV. With the Cs coating, however, the spectra have distinct low-energy absorption peaks below ∼1 eV indicating surface absorption and effective shrinkage of the band gap. Moreover, the intensity of these low-energy peaks is enhanced by the thickness of the Cs coating. These low-energy peaks arise due to the optical transitions among the metallic states of Cs-coated $CsPbX_3$ (X = I, Br). Observed changes in the absorption spectra in the energy range of 0−1.5 eV are concomitant with the lowering of the work function with a Cs coating on the $CsPbX_3$ (X = I, Br) surface.

Previous studies demonstrated that the inclusion of spin−orbit coupling (SOC) is important for the correct modeling of the electronic structure of halide perovskites containing Pb.[58] Its influence on the calculated work function, however, has not been established. To test this, we calculated the work function of the [001] surface of pure $CsPbI_3$. We found that neither the Fermi energy nor the vacuum potential changes in any significant way. E_{Fermi} increases by 0.033 eV, and E_{vacuum} decreases by 0.198 eV. This is not surprising as the Fermi energy in the pure systems is determined by the top of the valence band and it is the conduction band that is changed significantly when SOC is included. However, since the Fermi energy is shifted into the conduction band for cesiated systems, it is not obvious that SOC can be completely excluded in those cases. Consequently, we calculated the work function for the Cs-coated [001] surface of $CsPbI_3$ with[59] and without SOC and found that while both the Fermi energy and vacuum potential shifted (details in SI Table S2), the overall work function changes from 2.12 eV without SOC to 2.30 eV with SOC. This is less than a 200 meV difference and is well within the uncertainties of our study. The comparatively small change in work function with the inclusion of SOC is an indication that the calculated work function is not very sensitive to the level of theory used.

In addition to having a low work function and suitable optical properties, the material also has to be thermodynamically stable. The adsorption energy of Cs on the different surfaces reflects the overall stability of the systems investigated in this study. The adsorption energy of a Cs atom on the surface of the perovskite slab is computationally estimated as

$$E_{ads} = E_{total} - (E_{slab} + E_{Cs}) \quad (3)$$

where E_{total} is the energy of the entire system, E_{Slab} is the energy of the pristine perovskite slab, and E_{Cs} is the total energy of the Cs coating. With this convention, negative values indicate an exothermic process. This value is then divided by the number of Cs atoms coating the surface to obtain the energy per Cs atom. This allows for a better comparison of the single and dense coatings. These calculated results for adsorption energy are presented in Table 1. Here we see

Table 1. Adsorption Energy (eV) of Cs Coating on the [001] Surface for $CsPbX_3$

	$CsPbI_3$	$CsPbBr_3$
single coating	−0.47	−0.36
dense coating	−0.25	−0.17

that $CsPbI_3$ has not only a lower work function but also a slightly lower adsorption energy. This suggests its higher stability compared to the bromide perovskites when being coated with Cs.

To conclude, in this letter we examined the influence of the Cs coating on the work function of $CsPbX_3$ (X = I, Br). We found that introducing a Cs coating lowers the work function substantially from 3.9 to 4.7 to 1.8−2.3 eV depending on the participating halide and terminating surface. Specifically, we find that for pure perovskites, systems containing Br and being terminated with the [110] surface have the lowest work functions. However, once a Cs coating is added, systems containing I and terminated with a [001] surface have the lowest work functions. These results are in good agreement with the recent experimental demonstration of Cs-coated perovskite materials as photocathode devices,[37] and the insights gained here can further be used for material development. A phenomenological model was developed to predict the work function with the material, surface coverage, and surface termination. The density of states calculations show that adding a Cs coating raises the Fermi energy (and HOMO energy) into the conduction band, lowering the work function. A charge density calculation demonstrates that these new states within the band gap and below the new Fermi energy are attributed to the surface Cs atoms. The optical absorption further exhibits low-energy peaks supporting the surface optical activity of these coated perovskites. Altogether, this study aims to facilitate the further experimental develop-

https://doi.org/10.1021/acs.jpclett.1c01412
J. Phys. Chem. Lett. 2021, 12, 6269−6276

ment of Cs-coated halide perovskites as possible next-generation photocathode materials.

■ ASSOCIATED CONTENT

Supporting Information

The Supporting Information is available free of charge at https://pubs.acs.org/doi/10.1021/acs.jpclett.1c01412.

Computational methods; convergence tests of cutoff energy, K-point sampling, amount of vacuum, and slab thickness; cell design parameters and considerations; example plot of the planar averaged electrostatic potential; GL model derivation and Cs/W $CsPbBr_3$ GL results; $CsPbBr_3$ DOS(S9), [110] HOMO charge density plots, and optical absorption spectra; and Fermi energy, vacuum energy, and work function for the [001] surface of $CsPbI_3$ with and without spin−orbit coupling (PDF)

■ AUTHOR INFORMATION

Corresponding Authors

Sergei Tretiak − *Theoretical Division, Los Alamos National Laboratory, Los Alamos, New Mexico 87545, United States;* orcid.org/0000-0001-5547-3647; Email: serg@lanl.gov

Amanda J. Neukirch − *Theoretical Division, Los Alamos National Laboratory, Los Alamos, New Mexico 87545, United States;* orcid.org/0000-0002-6583-0086; Email: ajneukirch@lanl.gov

Authors

Sina G. Lewis − *Theoretical Division, Los Alamos National Laboratory, Los Alamos, New Mexico 87545, United States; Department of Physics, University of Colorado—Boulder, Boulder, Colorado 43210, United States*

Dibyajyoti Ghosh − *Theoretical Division and Center for Nonlinear Studies, Los Alamos National Laboratory, Los Alamos, New Mexico 87545, United States;* orcid.org/0000-0002-3640-7537

Kevin L. Jensen − *U.S. Naval Research Laboratory, Washington, D.C. 20375, United States*

Daniel Finkenstadt − *U.S. Naval Academy, Annapolis, Maryland 21402, United States*

Andrew Shabaev − *U.S. Naval Research Laboratory, Washington, D.C. 20375, United States*

Samuel G. Lambrakos − *U.S. Naval Research Laboratory, Washington, D.C. 20375, United States*

Fangze Liu − *Theoretical Division, Los Alamos National Laboratory, Los Alamos, New Mexico 87545, United States;* orcid.org/0000-0003-3114-5280

Wanyi Nie − *Theoretical Division, Los Alamos National Laboratory, Los Alamos, New Mexico 87545, United States;* orcid.org/0000-0002-5909-3155

Jean-Christophe Blancon − *Department of Chemical and Biomolecular Engineering, Rice University, Houston, Texas 77006, United States*

Liujiang Zhou − *Theoretical Division, Los Alamos National Laboratory, Los Alamos, New Mexico 87545, United States; Institute of Fundamental and Frontier, Sciences, University of Electronic Science and Technology of China, Chengdu 610054, P. R. China;* orcid.org/0000-0001-5814-4486

Jared J. Crochet − *Theoretical Division, Los Alamos National Laboratory, Los Alamos, New Mexico 87545, United States*

Nathan Moody − *Theoretical Division, Los Alamos National Laboratory, Los Alamos, New Mexico 87545, United States*

Aditya D. Mohite − *Department of Chemical and Biomolecular Engineering, Rice University, Houston, Texas 77006, United States;* orcid.org/0000-0001-8865-409X

Complete contact information is available at: https://pubs.acs.org/10.1021/acs.jpclett.1c01412

Notes

The authors declare no competing financial interest.

■ ACKNOWLEDGMENTS

The work at Los Alamos National Laboratory (LANL) was supported by the LANL LDRD program (S.G.L., F.L., W.N., A.J.N., and S.T.). This work was done in part at the Center for Nonlinear Studies (CNLS) and the Center for Integrated Nanotechnologies CINT), a U.S. Department of Energy and Office of Basic Energy Sciences user facility at LANL. This research used resources provided by the LANL Institutional Computing Program. LANL is operated by Triad National Security, LLC, for the National Nuclear Security Administration of the U.S. Department of Energy under contract no. 89233218NCA000001. D.F. acknowledges support from the Office of Naval Research and the NRL-USNA Cooperative Program for Scientific Interchange.

■ REFERENCES

(1) Jacobs, R.; Morgan, D.; Booske, J. Work Function and Surface Stability of Tungsten-Based Thermionic Electron Emission Cathodes. *APL Mater.* **2017**, *5*, 116105.

(2) Yue, G. Z.; Qiu, Q.; Gao, B.; Cheng, Y.; Zhang, J.; Shimoda, H.; Chang, S.; Lu, J. P.; Zhou, O. Generation of Continuous and Pulsed Diagnostic Imaging X-Ray Radiation Using a Carbon-Nanotube-Based Field-Emission Cathode. *Appl. Phys. Lett.* **2002**, *81*, 355−357.

(3) Massey, H. S. W. *Applied Atomic Collision Physics*; Academic Press: New York, 1982.

(4) Wang, G.; Pandey, R.; Moody, N. A.; Batista, E. R. Degradation of Alkali-Based Photocathodes from Exposure to Residual Gases: A First-Principles Study. *J. Phys. Chem. C* **2017**, *121*, 8399−8408.

(5) Xiang, R.; Teichert, J. Photocathodes for High Brightness Photo Injectors. *Phys. Procedia* **2015**, *77*, 58−65.

(6) Huang, P. W.; Huang, W. H.; Tang, C. X. Model of Photocathode for CW Electron Gun. In *38th International Free eElectron Laser Conference*; 2017; pp 386−388.

(7) Sheffield, R. L. MaRIE XFEL Scientific Requirements. In *Challenges of High Photon Energy, High-Repetition Rate XFELs*; 2016.

(8) Bazarov, I. V.; Dunham, B. M.; Liu, X.; Virgo, M.; Dabiran, A. M.; Hannon, F.; Sayed, H. Thermal Emittance and Response Time Measurements of a GaN Photocathode. *J. Appl. Phys.* **2009**, *105* (8), 083715.

(9) Chanlek, N.; Herbert, J. D.; Jones, R. M.; Jones, L. B.; Middleman, K. J.; Militsyn, B. L. The Degradation of Quantum Efficiency in Negative Electron Affinity GaAs Photocathodes Under Gas Exposure. *J. Phys. D: Appl. Phys.* **2014**, *47*, 055110.

(10) Shen, L.; Fang, Y.; Wang, D.; Bai, Y.; Deng, Y.; Wang, M.; Lu, Y.; Huang, J. A Self-Powered, Sub-Nanosecond-Response Solution-Processed Hybrid Perovskite Photodetector for Time-Resolved Photoluminescence-Lifetime Detection. *Adv. Mater.* **2016**, *28*, 10794−10800.

(11) Dowell, D. H.; Bazarov, I.; Dunham, B.; Harkay, K.; Hernandez-Garcia, C.; Legg, R.; Padmore, H.; Rao, T.; Smedley, J.; Wan, W. Cathode R&D for Future Light Sources. *Nucl. Instrum. Methods Phys. Res., Sect. A* **2010**, *622*, 685−697.

(12) Pérez Quintero, K. J.; Antipov, S.; Sumant, A. V.; Jing, C.; Baryshev, S. V. High Quantum Efficiency Ultrananocrystalline

Diamond Photocathode for Photoinjector Applications. *Appl. Phys. Lett.* **2014**, *105* (12), 123103.
(13) Jacobs, R.; Booske, J.; Morgan, D. Understanding and Controlling the Work Function of Perovskite Oxides Using Density Functional Theory. *Adv. Funct. Mater.* **2016**, *26*, 5471−5482.
(14) Yilmaz, P.; Yeo, D.; Loh, L.; Dunn, S. Perovskite BiFeO3 Thin Film Photocathode Performance with Visible Light Activity. *Nanotechnology* **2016**, *27*, 345402.
(15) Tabari, T.; Ebadi, M.; Singh, D.; Caglar, B.; Baris, Y. M. Efficient Synthesis of Perovskite-Type Oxide Photocathode by Nonhydrolytic Sol-Gel Method with an Enhanced Photoelectrochemical Activity. *J. Alloys Compd.* **2018**, *750*, 248−257.
(16) Díez-García, M.; Celorrio, V.; Calvillo, L.; Tiwari, D.; Gómez, R.; Fermín, D. J. YFeO\textsubscript{3} Photocathodes for Hydrogen Evolution. *Electrochim. Acta* **2017**, *246*, 365−371.
(17) Stranks, S. D.; Snaith, H. J. Metal-Halide Perovskites for Photovoltaic and Light-Emitting Devices. *Nat. Nanotechnol.* **2015**, *10*, 391−402.
(18) Li, Y.; Shi, Z.-F.; Lei, L.-Z.; Ji, H.-F.; Wu, D.; Xu, T.-T.; Tian, Y.-T.; Li, X.-J. High-Performance Perovskite Photodetectors Based on Solution-Processed All-Inorganic CsPbBr\textsubscript{3} Thin Films. *J. Mater. Chem. C* **2017**, *5*, 8355−8360.
(19) Dong, Y.; Gu, Y.; Zou, Y.; Song, J.; Xu, L.; Li, J.; Xue, J.; Li, X.; Zeng, H. Improving All-Inorganic Perovskite Photodetectors by Preferred Orientation and Plasmonic Effect. *Small* **2016**, *12*, 5622−5632.
(20) Song, J.; Li, J.; Li, X.; Xu, L.; Dong, Y.; Zeng, H. Quantum Dot Light-Emitting Diodes Based on Inorganic Perovskite Cesium Lead Halides (CsPbX3). *Adv. Mater.* **2015**, *27*, 7162−7167.
(21) Paul, T.; Chatterjee, B. K.; Maiti, S.; Sarkar, S.; Besra, N.; Das, B. K.; Panigrahi, K. J.; Thakur, S.; Ghorai, U. K.; Chattopadhyay, K. K. Tunable Cathodoluminescence Over the Entire Visible Window from All-Inorganic Perovskite CsPbX3 1D Architecture. *J. Mater. Chem. C* **2018**, *6*, 3322−3333.
(22) Stoumpos, C. C.; Malliakas, C. D.; Peters, J. A.; Liu, Z.; Sebastian, M.; Im, J.; Chasapis, T. C.; Wibowo, A. C.; Chung, D. Y.; Freeman, A. J.; et al. Crystal Growth of the Perovskite Semiconductor CsPbBr3: A New Material for High-Energy Radiation Detection. *Cryst. Growth Des.* **2013**, *13*, 2722−2727.
(23) Wang, C.; Chesman, A. S. R.; Jasieniak Jacek, J. Stabilizing the Cubic Perovskite Phase of CsPbI3 Nanocrystals by Using an Alkyl Phosphinic Acid. *Chem. Commun.* **2017**, *53*, 232−235.
(24) Shi, D.; Adinolfi, V.; Comin, R.; Yuan, M.; Alarousu, E.; Buin, A.; Chen, Y.; Hoogland, S.; Rothenberger, A.; Katsiev, K.; et al. Low Trap-State Density and Long Carrier Diffusion in Organolead Trihalide Perovskite Single Crystals. *Science (Washington, DC, U. S.)* **2015**, *347*, 519−522.
(25) Stoumpos, C. C.; Malliakas, C. D.; Kanatzidis, M. G. Semiconducting Tin and Lead Iodide Perovskites with Organic Cations: Phase Transitions, High Mobilities, and Near-Infrared Photoluminescent Properties. *Inorg. Chem.* **2013**, *52*, 9019−9038.
(26) Noh, J. H.; Im, S. H.; Heo, J. J.; Mandal, T. N.; Seok, S. Il. Chemical Management for Colorful, Efficient, and Stable Inorganic-Organic Hybrid Nanostructured Solar Cells. *Nano Lett.* **2013**, *13*, 1764−1769.
(27) Dirin, D. N.; Cherniukh, I.; Yakunin, S.; Shynkarenko, Y.; Kovalenko, M. V. Solution-Grown CsPbBr3 Perovskite Single Crystals for Photon Detection. *Chem. Mater.* **2016**, *28*, 8470−8474.
(28) Wei, Z.; Perumal, A.; Su, R.; Sushant, S.; Xing, J.; Zhang, Q.; Tan, S. T.; Demir, H. V.; Xiong, Q. Solution-Processed Highly Bright and Durable Cesium Lead Halide Perovskite Light-Emitting Diodes. *Nanoscale* **2016**, *8*, 18021−18026.
(29) Zhang, D.; Eaton, S. W.; Yu, Y.; Dou, L.; Yang, P. Solution-Phase Synthesis of Cesium Lead Halide Perovskite Nanowires. *J. Am. Chem. Soc.* **2015**, *137*, 9230−9233.
(30) Jeon, N. J.; Noh, J. H.; Yang, W. S.; Kim, Y. C.; Ryu, S.; Seo, J.; Seok, S. Il. Compositional Engineering of Perovskite Materials for High-Performance Solar Cells. *Nature* **2015**, *517*, 476−480.
(31) Zhou, H.; Chen, Q.; Li, G.; Luo, S.; Song, T. B.; Duan, H. S.; Hong, Z.; You, J.; Liu, Y.; Yang, Y. Interface Engineering of Highly Efficient Perovskite Solar Cells. *Science (Washington, DC, U. S.)* **2014**, *345*, 542−546.
(32) Kojima, A.; Teshima, K.; Shirai, Y.; Miyasaka, T. Organometal Halide Perovskites as Visible-Light Sensitizers for Photovoltaic Cells. *J. Am. Chem. Soc.* **2009**, *131*, 6050−6051.
(33) Kim, I. S.; Pellin, M. J.; Martinson, A. B. F. Acid-Compatible Halide Perovskite Photocathodes Utilizing Atomic Layer Deposited TiO2 for Solar-Driven Hydrogen Evolution. *ACS Energy Lett.* **2019**, *4*, 293−298.
(34) Zhang, H.; Yang, Z.; Yu, W.; Wang, H.; Ma, W.; Zong, X.; Li, C. A Sandwich-Like Organolead Halide Perovskite Photocathode for Efficient and Durable Photoelectrochemical Hydrogen Evolution in Water. *Adv. Energy Mater.* **2018**, *8*, 1800795.
(35) Gao, L.; Luo, W.; Yao, Y.; Zou, Z. All-Inorganic Lead Halide Photocathode for Stable Water Reduction. *Chem. Commun.* **2018**, *54*, 11459−11462.
(36) Crespo-Quesada, M.; Pazos-Outón, L. M.; Warnan, J.; Kuehnel, M. F.; Friend, R. H.; Reisner, E. Metal-Encapsulated Organolead Halide Perovskite Photocathode for Solar-Driven Hydrogen Evolution in Water. *Nat. Commun.* **2016**, *7*, 12555.
(37) Liu, F.; Sidhik, S.; Hoffbauer, M. A.; Lewis, S.; Neukirch, A. J.; Pavlenko, V.; Tsai, H.; Nie, W.; Even, J.; Tretiak, S.; et al. Highly Efficient Photoelectric Effect in Halide Perovskites for Regenerative Electron Sources. *Nat. Commun.* **2021**, *12*, 673.
(38) Karkare, S.; Boulet, L.; Singh, A.; Hennig, R.; Bazarov, I. Ab Initio Studies of Cs on GaAs (100) and (110) Surfaces. *Phys. Rev. B: Condens. Matter Mater. Phys.* **2015**, *91*, 035408.
(39) Diao, Y.; Liu, L.; Xia, S.; Feng, S.; Lu, F. The Electronic and Optical Properties of Cs Adsorbed GaAs Nanowires via First-Principles Study. *Phys. E* **2018**, *101*, 5−10.
(40) Sutton, R. J.; Eperon, G. E.; Miranda, L.; Parrott, E. S.; Kamino, B. A.; Patel, J. B.; Hörantner, M. T.; Johnston, M. B.; Haghighirad, A. A.; Moore, D. T.; et al. Bandgap-Tunable Cesium Lead Halide Perovskites with High Thermal Stability for Efficient Solar Cells. *Adv. Energy Mater.* **2016**, *6*, 1502458.
(41) Olthof, S. Research Update: The Electronic Structure of Hybrid Perovskite Layers and Their Energetic Alignment in Devices. *APL Mater.* **2016**, *4*, 091502.
(42) Luchkin, S. Y.; Akbulatov, A. F.; Frolova, L. A.; Tsarev, S. A.; Troshin, P. A.; Stevenson, K. J. Spatially-Resolved Nanoscale Measurements of Grain Boundary Enhanced Photocurrent in Inorganic CsPbBr3 Perovskite Films. *Sol. Energy Mater. Sol. Cells* **2017**, *171*, 205−212.
(43) Kim, Y. G.; Kim, T.-Y.; Oh, J. H.; Choi, K. S.; Kim, Y.-J.; Kim, S. Y. Efficiency of Ab-Initio Total Energy Calculations for Metals and Semiconductors Using a Plane-Wave Basis Set. *Phys. Chem. Chem. Phys.* **2017**, *19*, 6257−6263.
(44) Kulbak, M.; Gupta, S.; Kedem, N.; Levine, I.; Bendikov, T.; Hodes, G.; Cahen, D. Cesium Enhances Long-Term Stability of Lead Bromide-Based Solar Cells. *J. Phys. Chem. Lett.* **2016**, *7*, 167−172.
(45) Gyftopoulos, E.; Levine, J. Work Function Variation of Metals Coated by Metallic Films. *J. Appl. Phys.* **1962**, *33*, 67−73.
(46) Jensen, K. L. *Electron Emission Physics: Advances in Imaging and Electron Physics*; 2007.
(47) Jensen, K. L.; Shabaev, A.; Lambrakos, S. G.; Finkenstadt, D.; Petillo, J. J.; Alexander, A. M.; Smedley, J.; Moody, N. A.; Yamaguchi, H.; Liu, F.; et al. An Extended Moments Model of Quantum Efficiency for Metals and Semiconductors. *J. Appl. Phys.* **2020**, *128*, 015301.
(48) Zhong, Z.; Hansmann, P. Tuning the Work Function in Transition Metal Oxides and Their Heterostructures. *Phys. Rev. B: Condens. Matter Mater. Phys.* **2016**, *93*, 235116.
(49) Kresse, G.; Furthmüller, J. Efficiency of Ab-Initio Total Energy Calculations for Metals and Semiconductors Using a Plane-Wave Basis Set. *Comput. Mater. Sci.* **1996**, *6*, 15−50.

https://doi.org/10.1021/acs.jpclett.1c01412
J. Phys. Chem. Lett. 2021, 12, 6269−6276

(50) Kresse, G.; Furthmller, J. Efficient Iterative Schemes for Ab Initio Total-Energy Calculations Using a Plane-Wave Basis Set. *Phys. Rev. B: Condens. Matter Mater. Phys.* **1996**, *54*, 11169−11186.
(51) Kresse, G.; Joubert, D. From Ultrasoft Pseudopotentials to the Projector Augmented-Wave Method. *Phys. Rev. B: Condens. Matter Mater. Phys.* **1999**, *59*, 1758−1775.
(52) Perdew, J. P.; Burke, K.; Ernzerhof, M. Generalized Gradient Approximation Made Simple. *Phys. Rev. Lett.* **1996**, *77*, 3865−3868.
(53) Kittel, C. *Introduction to Solid State Physics*; 2007.
(54) Jensen, K.; Moody, N. A.; Feldman, D.; Montgomery, E.; PG, O. Photoemission from Metals and Cesiated Surfaces. *J. Appl. Phys.* **2007**, *102*, 074902.
(55) Moody, N. A.; Jensen, K. L.; Feldman, D. W.; O'Shea, P. G.; Montgomery, E. J. Prototype Dispenser Photocathode: Demonstration and Comparison to Theory. *Appl. Phys. Lett.* **2007**, *90*, 114108.
(56) Haas, G. A.; Thomas, R. E. *Techniques of Metals Research*; 1968; Part 1, Chapter 2, Vol. *VI*, pp 91−262.
(57) Gajdoš, M.; Hummer, K.; Kresse, G.; Furthmüller, J.; Bechstedt, F. Linear Optical Properties in the Projector-Augmented Wave Methodology. *Phys. Rev. B: Condens. Matter Mater. Phys.* **2006**, *73*, 045112.
(58) Katan, C.; Pedesseau, L.; Kepenekian, M.; Rolland, A.; Even, J. Interplay of Spin-Orbit Coupling and Lattice Distortion in Metal Substituted 3D Tri-Chloride Hybrid Perovskites. *J. Mater. Chem. A* **2015**, *3*, 9232−9240.
(59) Steiner, S.; Khmelevskyi, S.; Marsmann, M.; Kresse, G. Calculation of the Magnetic Anisotropy with Projected-Augmented-Wave Methodology and the Case Study of Disordered Fe1-XCox Alloys. *Phys. Rev. B: Condens. Matter Mater. Phys.* **2016**, *93*, 224425.

https://doi.org/10.1021/acs.jpclett.1c01412
J. Phys. Chem. Lett. 2021, 12, 6269−6276